Title

Physical, Biomechanical, and Optical Characterization of Collagen and Elastin Blend Hydrogels

Journal

Annals of Biomedical Engineering, 48(12)

ISSN

0090-6964

Authors

Vazquez-Portalatin, Nelda

Alfonso-Garcia, Alba

Liu, Julie C

et al.

Publication Date

2020-12-01

DOI

10.1007/s10439-020-02605-x

Peer reviewed

HHS Public Access

Author manuscript

Ann Biomed Eng. Author manuscript; available in PMC 2021 December 01.

Published in final edited form as:

Ann Biomed Eng. 2020 December ; 48(12): 2924–2935. doi:10.1007/s10439-020-02605-x.

Physical, biomechanical, and optical characterization of collagen and elastin blend hydrogels

Nelda Vazquez-Portalatin[1,2], **Alba Alfonso-Garcia**[1], **Julie C. Liu**[2,3], **Laura Marcu**[1], **Alyssa Panitch**[1,*]

[1]University of California, Davis, Biomedical Engineering Department, 451 Health Sciences Dr, Davis, CA, 95616, USA

[2]Purdue University, Weldon School of Biomedical Engineering, 206 S Martin Jischke Dr, West Lafayette, IN, 47907, USA

[3]Purdue University, Davidson School of Chemical Engineering, 480 Stadium Mall Dr, West Lafayette, IN, 47907, USA

Abstract

Collagen and elastin proteins are major components of the extracellular matrix of many organs. The presence of collagen and elastin networks, and their associated properties, in different tissues have led scientists to study collagen and elastin composites for use in tissue engineering. In this study, we characterized physical, biochemical, and optical properties of gels composed of collagen and elastin blends. We demonstrated that the addition of varying amounts of elastin to the constructs alters collagen fibrillogenesis, D-banding pattern length, and storage modulus. However, the addition of elastin does not affect collagen fibril diameter. We also evaluated the autofluorescence properties of the different collagen and elastin blends with fluorescence lifetime imaging (FLIm). Autofluorescence emission showed a red shift with the addition of elastin to the hydrogels. The fluorescence lifetime of the gels increased with the addition of elastin and were strongly correlated with the storage moduli measurements. These results suggest that FLIm can be used to monitor the gels' mechanical properties nondestructively. These collagen and elastin constructs, along with the FLIm capabilities, can be used to develop and study collagen and elastin composites for tissue engineering and regenerative medicine.

Keywords

fibrillogenesis; D-banding pattern; storage modulus; FLIm; autofluorescence lifetime

*Address all correspondence to: Alyssa Panitch, 451 Health Sciences Dr, GBSF Room 2303, Davis, CA, 95616, USA, Phone number: 530-754-3222, FAX number:, apanitch@ucdavis.edu.

Introduction

Collagen has been extensively used in tissue engineering due to its biocompatibility, abundant presence in body tissues, and wide clinical approval[5,21,25,26,28]. However, collagen constructs do not fully mimic the complex composition, network, and biochemical and biomechanical properties observed in native tissues[5]. Previous work has focused on the addition of other extracellular matrix (ECM) components, particularly elastin[6,11,15,18,31,45,48,55], chondroitin sulfate[15,17,20,57,60,61,63], and hyaluronic acid[32,47,48,57,63], to collagen-based constructs to develop more complex materials with stronger mechanical and biological properties that are reminiscent of native tissue composition and network organization.

Elastin is a structural protein present in connective, vascular, and load-bearing tissues[33,48,59] and has also been used in tissue engineering due to its elastic mechanical properties[18,54,67]. Collagen and elastin networks are present in the ECM of many organs including the skin, blood vessels, and lungs[33,54,59]. These matrix proteins provide different tissues with tensile strength and elasticity allowing them to resist deformation and repetitive stress[43]. Thus, collagen and elastin composites have been proposed for use in vascularization[6,7,9,48,67], wound repair[10,31,54,67], and the development of alveolar and lung replacements[18].

Measuring the physical, chemical, and biomechanical properties of hydrogels and other tissue surrogates is necessary to ensure controlled and reproducible scaffolds. Different preparation methods, such as 3D printing[44,46], uniform mixing[22], and pipetting[22], have been analyzed to determine the robustness and reliability of the output product. Besides fabrication parameters, quantitative characterization methods have also been proposed to assist in the design and study of collagen hydrogels as viable tissue mimics[2]. However, most of the current techniques such as enzyme-linked immunosorbent assays (ELISAs) and rheological measurements are time-consuming, damage the sample, or require specific sample preparation that compromises the practical use of the constructs. Instead, optical imaging and spectroscopic techniques are fast, preserve the sample's integrity, and require minimal to no sample preparation. These characteristics allow for repeated measurements over time and increased sample throughput. Light absorbance measurements are informative of gel formation kinetics and polymerization[2]. Multiphoton microscopy (TPEF: two-photon excited fluorescence and SHG: second harmonic generation) has been used to quantify the mechanical properties of collagen gels[52,53]. Raman spectroscopy has also been used to characterize the chemical structure of collagen hydrogels[27,38,40]. More recently, autofluorescence lifetime imaging (FLIm) was used for nondestructive quantification of crosslink formation in collagen hydrogels[58] and of self- assembled articular cartilage[24]. FLIm has also shown correlation with biomechanical properties and biochemical composition of collagen and elastin rich tissue structures such as the swine carotid artery[1] and vascular grafts made out of bovine pericardium[35].

Here, we evaluate the effects of elastin addition to collagen hydrogels by measuring collagen fibril formation and the biophysical and biomechanical properties of the final constructs. In addition, we assess the capabilities of FLIm to nondestructively characterize hydrogels

composed of different collagen to elastin ratios and correlate the imaging results with the biophysical and biomechanical results.

Materials and Methods

Gel Preparation.

Rat tail collagen type I with a neutralization solution was purchased from Advanced Biomatrix (San Diego, CA). Soluble elastin from bovine neck ligament was purchased from Elastin Products Company, Inc (Owensville, MO). Stock collagen solutions were prepared on ice by combining 1 part of the neutralizing solution and 9 parts of the collagen type I solution for the desired volume. Stock elastin solutions were prepared in 1x PBS at a concentration of 100 mg/mL. The stock collagen and elastin solutions were used to prepare collagen type I:elastin mixtures with ratios of 1:0 C (control), 1:0.5, 1:1, 1:1.5, 1:2, and 1:5 (Table 1). The collagen and elastin mixtures were dispensed into 8 mm diameter silicone molds, which were sandwiched between two glass slides. The mixtures were then incubated overnight at 37°C and 5% CO_2. The gels were stored in 1x PBS for a day at 4°C before measuring their mechanical properties.

Fibrillogenesis Assay.

Collagen and elastin hydrogel mixtures (n = 9) were prepared on ice and diluted 1:10 in 1x PBS for the fibrillogenesis assay. Samples of 200 μL were dispensed into 96-well plates, and the fibrillogenesis of the samples was measured as described previously[49]. Briefly, the turbidity of the samples was monitored by absorbance measurements at 313 nm every 45 s for 3 h in a SpectraMax M5 spectrophotometer set at 37°C (Molecular Devices, San Jose, CA). Absorbance measurements obtained from the collagen and elastin solutions were normalized to the values obtained from a standard solution of elastin in 1x PBS to remove any contributing autofluorescence from elastin.

Transmission Electron Microscopy (TEM).

A subset (1:0 C, 1:1, and 1:5, n = 3/group) of the collagen and elastin hydrogel solutions were prepared on ice and diluted 1:10 in 1x PBS. Samples of 7 μL were added to 200 mesh copper-coated grids and allowed to settle for 10 min. The sample excess was removed and 10 μL of a 2% uranyl acetate stain were added and removed immediately. A Talos L120C transmission electron microscope (FEI, Hillsboro, OR) was used to image the samples after allowing them to air dry.

Collagen D-banding patterns ($n \geq 46$), which are composed of overlap (dark bands) and gap regions (light bands), are produced when tropocollagen molecules are organized in a staggered formation[3,4,12,42]. These patterns were measured from the TEM images using ImageJ software (National Institutes of Health, Bethesda, MD). A parallel line was drawn along a fibril, over a light and a dark band, to obtain a measurement. ImageJ software was also used to measure the fibril diameter ($n \geq 46$) as described previously[63].

Rheological Measurements.

A DHR-3 rheometer (TA Instruments, New Castle, DE) was used to perform rheological analysis with an 8 mm crosshatched plate geometry. Gels ($n \geq 16$) were placed on a crosshatched bottom plate surrounded by 1x PBS to prevent dehydration. Temperature sweeps were performed from 20°C to 40°C with a frequency of 0.1 Hz and a controlled stress of 0.3 Pa.

Autofluorescence measurements.

The gel autofluorescence emission at 355 nm excitation with 5 nm step size was measured in a SpectraMax M5 spectrophotometer (Molecular Devices, San Jose, CA).

Fluorescence lifetime imaging (FLIm) was performed with a fiber-based multispectral time-resolved fluorescence instrument that is described elsewhere[65]. The FLIm instrument used a pulse sampling technique to retrieve autofluorescence spectral and lifetime properties from samples exposed to 355 nm pulsed laser light (pulse duration < 0.6 ns, pulse energy > 2 μJ, repetition rate 4kHz; TEEM photonics STV-02E, Meylan, France). A multimode fiber (400 μm core diameter) was raster scanned across the surface of the samples with a 3-axis translation stage (PROmech LP28, Parker, Charlotte, NC) to generate the images. Autofluorescence from the hydrogels was collected back through the same multimode fiber and detected on three spectral bands or channels (Ch1: 390/18 nm, Ch2: 435/40 nm, and Ch3: 542/20 nm) connected to a microchannel plate photomultiplier tube (MCP-PMT; R3809U-50, Hamamatsu, Japan) and a high speed digitizer (12.5 GS/s, 3 GHz bandwidth; NI PXIe-5185, National Instruments, Austin, TX). The instrument response function was measured after each imaging session using the decay of 2-DASPI (2-[4-(dimethylamino)styryl]-1-methylpyridinium iodide; Sigma-Aldrich), with an average fluorescence lifetime of 34 ps when dissolved in ethanol[37].

Images sized ~ 30 mm × 12 mm were acquired with square pixels of 200 μm × 200 μm in about 2 minutes. Each image consisted of three replicates of 8 mm gels. FLIm parameters were obtained from the acquired fluorescence decay waveforms by applying a constrained least square deconvolution with expansion into the Laguerre basis functions[30]. Finally, the average fluorescence lifetime (τ_{avg}) was calculated as the expectation value of the probability density function of the fluorescence decay (eq. 1) for each spectral band as follows:

$$\tau_{avg} = \frac{\int_0^\infty t \cdot I(t)dt}{\int_0^\infty I(t)dt} \quad (1)$$

Reported metrics indicate the mean and the standard deviation of all the pixels from replicate gels obtained within a circular region delineating each gel.

Statistical Analysis.

Results are represented as a mean with error bars corresponding to the standard deviation. Statistical analysis was performed using GraphPad Prism (GraphPad Software, San Diego,

CA) with $\alpha = 0.05$, and significance was determined with p-value < 0.05. All results were analyzed using single factor analysis of variance (ANOVA) and Tukey's *post hoc* tests or Dunnett's multiple comparisons tests. Nonparametric Kendall τ_b correlation analyses were performed using SPSS Statistics (IBM, Armonk, NY) with $\alpha = 0.05$. Significance was determined with p-value < 0.05.

Results

Elastin increases fibrillogenesis.

Turbidity measurements of the collagen and elastin solutions for the different blends (1:0 C, 1:0.5, 1:1, 1:1.5, 1:2, and 1:5) showed that the addition of elastin increased the sample absorbance at 313 nm after 1000 s when compared to a collagen only solution (1:0 C) (Figure 1) and suggest an increase in fibrillogenesis. Common turbidity measurements, such as total change in absorbance (Δabsorbance) and halftime ($t_{1/2}$), were calculated to better quantify the sample polymerization[2] (Table 2). The addition of elastin caused a 37% increase or more in total change in absorbance when compared to the control group. All of the collagen and elastin blend gel solutions showed a significantly higher total change in absorbance than control but were not significantly different from each other. No significant differences were observed when comparing the halftime measurements for the gel blend solutions with the 1:0 control.

Elastin addition decreases the collagen D-banding pattern but does not affect collagen fibril diameter.

TEM images were used to measure the D-banding pattern (a light and a dark band) and fibril diameter of collagen fibrils present in a subset (1:0 C, 1:1, and 1:5) of the collagen and elastin blend hydrogels (Figure 2). This subset of conditions was used to verify that collagen fibrils were forming within our hydrogels and that their D-banding pattern remained consistent with that observed in nature. Compared to the D-banding pattern length observed in the control gels, the 1:5 collagen and elastin solutions showed a significant decrease of 0.85 nm in the D-banding pattern observed in the collagen fibrils (Table 3). No significant difference was observed between the 1:0 C and 1:1 collagen and elastin blends.

The fibril diameter of the collagen fibrils present in the collagen and elastin solutions was measured from the TEM images (Figure 2). The results obtained showed no significant differences among the collagen and elastin blends, 1:1 and 1:5, and control (Table 3). Table 3 shows the average fibril diameter, standard deviation, and p values for fibrils present in the 1:0 C, 1:1, and 1:5 gels.

Addition of elastin decreases storage modulus.

All of the collagen and elastin gels showed significantly lower storage moduli from the control (1:0 C) gels by at least 14.6 Pa, except for the 1:0.5 collagen to elastin blend (Figure 3 and Table 4). Figure 3B shows the loss moduli values for the different gel types. The observed loss moduli measurements (Figure 3B) are lower than their corresponding storage moduli measurements (Figure 3A) indicating our hydrogels mainly behave as elastic materials.

Autofluorescence parameters react to the addition of elastin.

The emission spectra of the hydrogels (1:0.5, 1:1, 1:1.5, 1:2, and 1:5) upon 355 nm excitation are depicted in Figure 4A, together with the emission spectra of dry collagen type I flakes and elastin powder, for reference. With respect to the collagen spectrum, the emission from the hydrogels is increasingly red-shifted the more elastin is present in the blends.

The hydrogel fluorescence lifetime was measured in three spectral channels with the fiber-based FLIm system. Figure 4C displays the fluorescence lifetime maps from three gels in representative groups: control (1:0 C), 1:1, and 1:5. The brightness of the image indicates the intensity of the fluorescence, and the color indicates the τ_{avg}. Note that the hydrogels with the same formulation exhibit a uniform fluorescence lifetime. The addition of elastin lengthened the fluorescence lifetime of the gels in all spectral channels (Table 5). Compared to the control group, addition of elastin to a 1:0.5 ratio caused a rise of 0.90 ns, 0.53 ns, and 0.56 ns in channels 1 (390/18 nm), 2 (435/40 nm), and 3 (542/20 nm), respectively (Figure 4B). As the collagen to elastin ratio decreased from 1:0.5 to 1:5, the overall increase in fluorescence lifetime was of about 200 ps in every channel (Figure 4B, insert). Also for every channel, the lifetime values for the different gel types were all significantly different from one another.

Kendall τ_b correlation analysis.

The Kendall τ_b correlation test[35,36] was performed to assess the correlation between the FLIm measurements and the fibrillogenesis and storage modulus of the different gels. Figure 5 shows the Kendall τ_b coefficients and the p-values for the various correlation graphs. Following the Cohen standard[13] to evaluate the strength of the correlations, the results showed a significant and strong negative correlation between the lifetime measurements obtained for channels 2 and 3 and the storage modulus (τ_b: −0.733, p-value: 0.039, Figure 5B, and τ_b: −0.733, p-value: 0.039, Figure 5C, respectively). These results indicate a decrease in lifetime for channels 2 and 3 when the storage modulus increases. The changes observed differed in channel 1, the control sample with the largest storage modulus also had a significantly shorter lifetime, but the overall correlation resulted non-significant because the elastin-containing gels had undistinguishable lifetime values. This result links the fluorescence from elastin, rather than the collagen network itself, with the mechanical properties of the hydrogels. Changes in the structural microenvironment that occur upon addition of elastin may be responsible for both the change in lifetime and the decrease of the storage modulus. No other significant correlations were found between the lifetime and Δabsorbance measurements or the lifetime and halftime ($t_{1/2}$) measurements.

Discussion

In the work presented here, we characterized gels composed of collagen and elastin blends to better understand the effect of elastin addition to collagen constructs on the physical, biomechanical, and optical properties. First, collagen fibril formation was measured turbidimetrically[16,49] to determine whether elastin addition to collagen affects fibrillogenesis. Previous studies have shown that addition of molecules to collagen solutions

can alter the rate of fibril formation[49]. To further characterize the collagen fiber physical properties, we performed TEM imaging on a subset of the collagen and elastin gel blend solutions (1:0 C, 1:1, and 1:5) (Figure 2). With these images, we also analyzed the fibril diameter of the collagen fibrils.

Our findings demonstrated that addition of elastin to collagen gel solutions increased Δabsorbance at 313 nm (Figure 1 and Table 2) suggesting an increase in fibrillogenesis. Fibrillogenesis has been previously used to indicate fibril diameter changes when compared with control solutions[49]. According to that study, an increase in fibrillogenesis could indicate a larger fibril diameter. In other words, the addition of elastin to the collagen solutions could promote the formation of fibrils with larger diameters. However, our TEM analysis showed a collagen fibril diameter range of 68.90 – 72.32 nm that was not affected by the addition of elastin (Table 3). The increase in optical density that we observed could alternatively suggest that the addition of elastin results in molecular crowding, or aggregation of the collagen molecules, nucleation, and rapid fibril formation. This mechanism has been proposed for collagen and glycosaminoglycan constructs[50]. From the fibrillogenesis data, we also quantified the polymerization halftime, that is the time at which half of the total change in absorbance was achieved[2]. However, these data showed no difference in gelling time for the different collagen and elastin blends, that is no difference in the rate of fibrillogenesis (Table 2). The increase in Δabsorbance observed could be attributed to an increase in the total protein content within the blend gels leading to an increased network density compared to the collagen only controls. Collagen fibril formation involves interchain H-bonds that stabilize tropocollagen molecules allowing them to covalently crosslink with one another to form collagen fibrils[4]. Additionally, lysyl oxidase causes collagen to undergo hydroxypyridinium crosslinking via allysine and hydroxyallysine pathways[19]. Elastin fibrils are formed by desmosine and isodesmosine crosslinks facilitated by lysyl oxidase via allysine and lysine residues[19]. Even though lysyl oxidase causes collagen and elastin to form crosslinks, this enzyme is not present in our hydrogels and is not able to facilitate the formation of crosslinks between our collagen and elastin. The suggested increased network density could be the result of an increase in ionic and hydrogen bonds between collagen and elastin fibrils with elastin addition. The presence of diluted crosslinked monomers copurified, during the protein isolation process, with the uncrosslinked monomers used to prepare these hydrogels could provide a limited contribution to the increased network density. Nevertheless, the addition of elastin to the collagen constructs did not inhibit fibrillogenesis.

Using the TEM images, we also measured the D-banding pattern length associated with collagen fibrils. The D-banding pattern is a repeating pattern characteristic of fibrillar collagen with D-periodicity in the range of 64 – 67 nm[3,12,21,42]. Our results showed that 1:0 C and 1:1 collagen and elastin blends had statistically similar average D-banding patterns of 68.15 nm and 68.25 nm, respectively (Table 3). The 1:5 solutions had a significantly smaller average D-banding pattern of 67.30 nm. The significant decrease observed between the D-banding pattern of the 1:0 C (68.15 nm) and 1:5 (67.30 nm) hydrogels suggests that increasing elastin concentrations affects D-banding pattern length. The D-banding pattern shortening observed in our results could be caused by the co-assembly of collagen and elastin molecules into heterotypic fibrils. Studies have shown a decrease in D-banding

pattern length with the co-assembly of collagen type I and III when compared to collagen type I only hydrogels[3].These observed changes in D-banding pattern length are independent from fibril diameter measurements, and these results are consistent with previous work focused on collagen only solutions[8]. Previous studies have also shown that different tissues containing collagen fibrils, such as mouse cementum, skin, rat tail tendon, and periodontal ligament, exhibit a distribution of D-banding pattern length ranging from 62.4 – 68 nm[51]. Additionally, other studies have proposed that D-banding spacing changes as a function of strain and location within a ligament[34]. These findings suggest D-banding pattern length changes according to tissue function and could potentially be involved in modulating cellular responses.

While the decrease in D-banding pattern length observed with elastin addition could be advantageous when developing collagen and elastin hydrogels for specific tissues that have exhibited varying D-banding pattern lengths, differences observed in D-banding pattern size in our control gels and previous studies could be attributed to the manipulation of the samples such as the air-drying process involved in the TEM sample setup[29], which can cause the spacing in the fibrils to increase or decrease[56]. These limitations, along with the TEM resolution, should be acknowledged and considered when studying D-banding pattern lengths further.

We then performed rheological measurements to study the mechanical properties of the collagen and elastin blend hydrogels. These measurements determined that, while the initial addition of elastin in the 1:0.5 hydrogels did not affect the storage modulus, the increased addition of elastin observed in the 1:1, 1:1.5, 1:2, and 1:5 gels decreased their storage moduli and resulted in less stiff hydrogels. Similarly, Nguyen et al. detected a decrease in strength and stiffness with the addition of elastin to collagen fibers[45]. However, Berglung et al. and Bax et al. saw increases in stiffness in collagen and elastin constructs when compared to collagen only constructs[5,6]. These contrasting results could be attributed to several factors such as the enzymes (alpha-amylase, trypsin, collagenase)[14,23] and the isolation process[41] used to obtain the elastin product, the elastin solubility (soluble vs insoluble)[5], the scaffold fabrication process[2,5,6], the concentration of elastin[15] and crosslinking agents, such as 1-ethyl-3-(3-dimethyl aminopropyl)carbodiimide (EDC)[15], used to synthesize the hydrogels, as well as the different methods used to measure the mechanical properties[2,6,58]. While the modulatory effects of mechanical properties on cellular outcomes have been extensively studied and increased stiffness has been correlated with positive cell behavior, previous studies have shown that, although addition of elastin to collagen films can result in a reduction of the material's stiffness, the incorporation of elastin can improve cell attachment, spreading, and proliferation for cells with elastin-binding domains when compared to collagen only films[5].

Finally, we evaluated the autofluorescence properties of the hydrogel blends. Emission upon 355 nm excitation red-shifted with increasing amounts of elastin. These shifts could potentially be used to quantify the collagen to elastin ratio in a given hydrogel. Similarly, autofluorescence lifetime increased with decreasing collagen to elastin ratio in all tested spectral channels. Autofluorescence lifetime is independent from the fluorophore concentration, but it reflects changes in the fluorophore microenvironment. Conformational

changes and interaction with other molecules induce changes in the fluorophore's lifetime. The collagen to elastin ratio is poised to alter the local environment of the fluorophores present in collagen and elastin through changes in intra- and inter-molecular bonds. Previous studies on tissue samples also found longer lifetimes associated with decreased collagen to elastin ratios in the arterial wall[1] (excitation at 355 nm) and the eye[36] (excitation at 365 nm). It must be noted, however, that the fluorescence lifetime properties of hydrogels and mature tissue are expected to vary significantly. Multiple variables affect the fluorescence properties of the sample. Among others, we must consider tissue type, fiber assembly mechanism, pH, and degree of hydration. The collagen and elastin hydrogel blends here presented exhibit an autofluorescence emisison dominated by the fluorescence of elastin that has a higher quantum yield than collagen in this form. Instead, collagen autofluorescence in mature tissue is stronger, likely due to the presence of mature hydroxypyridinium fluorescent crosslinks, not likely present in the hydrogel assembly, and that also vary between tissue type (skin, bone, cartilage, etc)[39].

The FLIm results were correlated with the physical and biomechanical properties measured within this study. We found that the autofluorescence lifetime in two measured spectral bands (channels 2 and 3 that capture elastin fluorescence) were negatively correlated with the storage moduli. The correlation is possibly due to the structural changes in the microevironment of the gel network upon the addition of new elastin molecules. Such microenvironmental arrangements would affect both the mechanical properties of the gels and the fluorescence lifetime of the fluorophores present. This result encourages the use of fluorescence lifetime as an indirect measurement of the gels' mechanical properties. No other significant correlation were found between the autofluorescence lifetime and the fibrillogenesis parameters. Previous FLIm work in hydrogels already showed a correlation between the fluorescence lifetime and the storage moduli of a collection of glutaraldehyde crosslinked collagen hydrogels[58]. Additionally, the same approach was used to evaluate the mechanical properties of the degrading ECM of a collagenous tissue[35]. Together, these results further encourage the use of FLIm as a nondestructive tool for quantification of biomechanical properties of gels and engineered tissues. It is important to monitor and control biomechanical and biochemical properties during the fabrication of scaffolds to ensure reproducibility and reliability. Mechanical cues are also essential to direct cell behavior and development in hydrogels for use in tissue regeneration[62,64]. Thus, a nondestructive technique like FLIm would be useful to monitor mechanical cues *in vitro* and could serve as quality control when examining the mechanical properties of cell-embeded hydrogels throughout experiments. Using nondestructive imaging techniques for this purpose will reduce material cost and save time.q

In conclusion, we characterized hydrogels composed of collagen and elastin blends to elucidate their unique properties. We demonstrated that the addition of varying amounts of elastin to collagen affects hydrogel absorbance when studying fibrillogenesis, but does not affect fibril diameter. We observed a significant decrease in D-banding pattern length of the collagen fibrils, but D-banding pattern length measurements have limitations that need to be studied further. The storage modulus of the hydrogels is also affected by the addition of elastin. The hydrogel autofluorescence is also impacted by the collagen to elastin ratio, both in spectral emission (red-shifted with increased elastin content) and their autofluorescence

lifetime, which correlated with the storage moduli of the measured gels. The work presented here serves as a deeper understanding of how varying amounts of elastin affect collagen constructs. Additionally, this work encourages the use of FLIm as a quality control tool able to monitor hydrogel mechanical properties that will be important to influence cell behavior and development. This knowledge will prove useful when developing collagen and elastin constructs for tissue engineering applications in regenerative medicine in the future.

Acknowledgments

This work is supported by the National Institutes of Health Grants (R01 HL121068, R01 AR065398).

References

1. Alfonso-Garcia A, Haudenschild AK, and Marcu L. Label-free assessment of carotid artery biochemical composition using fiber-based fluorescence lifetime imaging. Biomed. Opt. Express 9:4064–4076, 2018. [PubMed: 30615748]
2. Antoine EE, Vlachos PP, and Rylander MN. Review of collagen I Hydrogels for bioengineered tissue microenvironments: characterization of mechanics, structure, and transport. Tissue Eng., Part B 20:683–696, 2014.
3. Asgari M, Latifi N, Heris HK, Vali H, and Mongeau L. In vitro fibrillogenesis of tropocollagen type III in collagen type i affects its relative fibrillar topology and mechanics. Sci. Rep 7:1–10, 2017. [PubMed: 28127051]
4. Aziz J, Shezali H, Radzi Z, Yahya NA, Abu Kassim NH, Czernuszka J, and Rahman MT. Molecular mechanisms of stress-responsive Changes in collagen and elastin networks in skin. Skin Pharmacol. Physiol 29:190–203, 2016. [PubMed: 27434176]
5. Bax DV, Smalley HE, Farndale RW, Best SM, and Cameron RE. Cellular response to collagen-elastin composite materials. Acta Biomater. 86:158–170, 2019. [PubMed: 30586647]
6. Berglund JD, Nerem RM, and Sambanis A. Incorporation of intact elastin scaffolds in tissue-engineered collagen-based vascular grafts. Tissue Eng. 10:1526–1535, 2004. [PubMed: 15588412]
7. Boland ED, Matthews JA, Pawlowski KJ, Simpson DG, Wnek GE, and Bowlin GL. Electrospinning collagen and elastin: preliminary vascular tissue engineering. Front. Biosci 9:1422–1432, 2004. [PubMed: 14977557]
8. Bozec L, van der Heijden G, and Horton M. Collagen fibrils: nanoscale ropes. Biophys. J 92:70–75, 2007. [PubMed: 17028135]
9. Calogero F, Palumbo FS, Pitarresia G, Allegra M, Pulei R, and Giammona G. Hyaluronic acid and α-elastin based hydrogel for three dimensional culture of vascular endothelial cells. J. Drug Deliv. Sci. Technol 46:28–33, 2018.
10. Castaño O, Pérez-Amodio S, Navarro-Requena C, Mateos-Timoneda MÁ, and Engel E. Instructive microenvironments in skin wound healing: Biomaterials as signal releasing platforms. Adv. Drug Deliv. Rev 129:95–117, 2018. [PubMed: 29627369]
11. De Chalain T, Phillips JH, and Hinek A. Bioengineering of elastic cartilage with aggregated porcine and human auricular chondrocytes and hydrogels containing alginate, collagen, and κ-elastin. J. Biomed. Mater. Res 44:280–288, 1999. [PubMed: 10397930]
12. Chapman A The Staining Pattern of Collagen Fibrils. J. Biol. Chem 254:10710–10714, 1979. [PubMed: 91606]
13. Cohen J Statistical Power Analysis for the Behavioral Sciences. Mawhaw: Lawrence Erlbaum Associates, 1988, 1–579 pp.
14. Daamen WF, Hafmans T, Veerkamp JH, and Van Kuppevelt TH. Comparison of five procedures for the purification of insoluble elastin. Biomaterials 22:1997–2005, 2001. [PubMed: 11426877]
15. Daamen WF, Van Moerkerk HTB, Hafmans T, Buttafoco L, Poot AA, Veerkamp JH, and Van Kuppevelt TH. Preparation and evaluation of molecularly-defined collagen-elastin-glycosaminoglycan scaffolds for tissue engineering. Biomaterials 24:4001–4009, 2003. [PubMed: 12834595]

16. Douglas T, Heinemann S, Bierbaum S, Scharnweber D, and Worch H. Fibrillogenesis of collagen types I, II, and III with small leucine-rich proteoglycans decorin and biglycan. Biomacromolecules 7:2388–2393, 2006. [PubMed: 16903686]
17. Douglas T, Heinemann S, Mietrach C, Hempel U, Bierbaum S, Scharnweber D, and Worch H. Interactions of collagen types I and II with chondroitin sulfates A-C and their effect on osteoblast adhesion. Biomacromolecules 8:1085–1092, 2007. [PubMed: 17378603]
18. Dunphy SE, Bratt JA, Akram KM, Forsyth NR, and El Haj AJ. Hydrogels for lung tissue engineering: biomechanical properties of thin collagen-elastin constructs. J. Mech. Behav. Biomed. Mater 38:251–259, 2014. [PubMed: 24809968]
19. Eyre DR, Paz MA, and Gallop PM. Cross-linking in collagen and elastin. Annu. Rev. Biochem 53:717–748, 1984. [PubMed: 6148038]
20. Gao Y, Li B, Kong W, Yuan L, Guo L, Li C, Fan H, Fan Y, and Zhang X. Injectable and self-crosslinkable hydrogels based on collagen type II and activated chondroitin sulfate for cell delivery. Int. J. Biol. Macromol 118:2014–2020, 2018. [PubMed: 30009919]
21. Gautieri A, Vesentini S, Redaelli A, and Buehler MJ. Hierarchical structure and nanomechanics of collagen microfibrils from the atomistic scale up. Nano Lett. 11:757–766, 2011. [PubMed: 21207932]
22. Gering C, Koivisto JT, Parraga JE, and Kellomäki M. Reproducible preparation method of hydrogels for cell culture applications-case study with spermidine crosslinked gellan gum. IFMBE Proc. 1-4, 2017.
23. Halabi CM, and Mecham RP. “Elastin purification and solubilization” In: Methods in Cell Biology, edited by Mecham RP. Cambridge: Academic Press Inc., 2018, pp. 207–222.
24. Haudenschild AK, Sherlock BE, Zhou X, Hu JC, Leach JK, Marcu L, and Athanasiou KA. Non-destructive detection of matrix stabilization correlates with enhanced mechanical properties of self-assembled articular cartilage. J. Tissue Eng. Regen. Med 13:637–648, 2019. [PubMed: 30770656]
25. Huang BJ, Hu JC, and Athanasiou KA. Cell-based tissue engineering strategies used in the clinical repair of articular cartilage. Biomaterials 98:1–22, 2016. [PubMed: 27177218]
26. Hunziker EB Articular cartilage repair: basic science and clinical progress. A review of the current status and prospects. Osteoarthr. Cartil 10:432–463, 2002.
27. Hwang YJ, and Lyubovitsky JG. The structural analysis of three-dimensional fibrous collagen hydrogels by raman microspectroscopy. Biopolymers 99:349–356, 2013. [PubMed: 23529687]
28. Irawan V, Sung T-C, Higuchi A, and Toshiyuki I. Collagen scaffolds in cartilage tissue engineering and relevant approaches for future development. Tissue Eng. Regen. Med 15:673–697, 2018. [PubMed: 30603588]
29. Jastrzebska M, Tarnawska D, Wrzalik R, Chrobak A, Grelowski M, Wylegala E, Zygadlo D, and Ratuszna A. New insight into the shortening of the collagen fibril D-period in human cornea. J. Biomol. Struct. Dyn 35:551–563, 2017. [PubMed: 26872619]
30. Jo JA, Fang Q, Papaioannou T, and Marcu L. Fast model-free deconvolution of fluorescence decay for analysis of biological systems. J. Biomed. Opt 9:743–752, 2004. [PubMed: 15250761]
31. Killat J, Reimers K, Choi CY, Jahn S, Vogt PM, and Radtke C. Cultivation of keratinocytes and fibroblasts in a three-dimensional bovine collagen-elastin matrix (Matriderm®) and application for full thickness wound coverage in vivo. Int. J. Mol. Sci 14:14460–14474, 2013. [PubMed: 23852021]
32. Kontturi L-S, Järvinen E, Muhonen V, Collin EC, Pandit AS, Kiviranta I, Yliperttula M, and Urtti A. An injectable, in situ forming type II collagen/hyaluronic acid hydrogel vehicle for chondrocyte delivery in cartilage tissue engineering. Drug Deliv. Transl. Res 4:149–158, 2014. [PubMed: 25786729]
33. Kristensen JH, and Karsdal MA. “Elastin” In: Biochemistry of Collagens, Laminins and Elastin: Structure, Function and biomarkers, edited by Karsdal MA. Cambridge: Academic Press Inc., 2016, pp. 197–201.
34. Kukreti U, and Belkoff SM. Collagen fibril D-period may change as a function of strain and location in ligament. J. Biomech 33:1569–1574, 2000. [PubMed: 11006380]

35. Li C, Shklover J, Parvizi M, Sherlock BE, Alfonso Garcia A, Haudenschild AK, Griffiths LG, and Marcu L. Label-free assessment of collagenase digestion on bovine pericardium properties by fluorescence lifetime imaging. Ann. Biomed. Eng 46:1870–1881, 2018. [PubMed: 30003502]
36. Liu R, Zhao Z, Zou L, Fang Q, Chen L, Argento A, and Lo JF. Compact, non-invasive frequency domain lifetime differentiation of collagens and elastin. Sensors Actuators B Chem. 219:283–293, 2015.
37. Ma D, Bec J, Yankelevich DR, Gorpas D, Fatakdawala H, and Marcu L. Rotational multispectral fluorescence lifetime imaging and intravascular ultrasound: bimodal system for intravascular applications. J. Biomed. Opt 19:066004, 2014. [PubMed: 24898604]
38. Manickavasagam A, Hirvonen LM, Melita LN, Chong EZ, Cook RJ, Bozec L, and Festy F. Multimodal optical characterisation of collagen photodegradation by femtosecond infrared laser ablation. Analyst 139:6135– 6143, 2014. [PubMed: 25318007]
39. Marcu L, Cohen D, Maarek J-MI, and Grundfest WS. Characterization of type I, II, III, IV, and V collagens by time-resolved laser-induced fluorescence spectroscopy. Proc. SPIE 3917, Optical Biopsy III 2000.
40. Martinez MG, Bullock AJ, MacNeil S, and Rehman IU. Characterisation of structural changes in collagen with Raman spectroscopy. Appl. Spectrosc. Rev 54:509–542, 2019.
41. Mecham RP Methods in elastic tissue biology: elastin isolation and purification. Methods 45:32–41, 2008. [PubMed: 18442703]
42. Miller A Molecular packing in collagen fibrils. Trends Biochem. Sci 7:13–18, 1982.
43. Muiznieks LD, and Keeley FW. Molecular assembly and mechanical properties of the extracellular matrix: A fibrous protein perspective. Biochim. Biophys. Acta 1832:866–875, 2013. [PubMed: 23220448]
44. Murphy SV, and Atala A. 3D bioprinting of tissues and organs. Nat. Biotechnol 32:773–785, 2014. [PubMed: 25093879]
45. Nguyen T-U, Bashur CA, and Kishore V. Impact of elastin incorporation into electrochemically aligned collagen fibers on mechanical properties and smooth muscle cell phenotype. Biomed. Mater 11:025008, 2016. [PubMed: 26987364]
46. Noh I, Kim N, Tran HN, Lee J, and Lee C. 3D printable hyaluronic acid-based hydrogel for its potential application as a bioink in tissue engineering. Biomater. Res 23:3, 2019. [PubMed: 30774971]
47. Novak T, Voytik-Harbin SL, and Neu CP. Cell encapsulation in a magnetically aligned collagen – GAG copolymer microenvironment. Acta Biomater. 11:274–282, 2015. [PubMed: 25257315]
48. Numata K, and Kaplan DL. “Biologically derived scaffolds” In: Advanced Wound Repair Therapies, edited by Farrar D. Philadelphia: Woodhead Publishing Limited, 2011, pp. 524–551.
49. Paderi JE, and Panitch A. Design of a synthetic collagen-binding peptidoglycan that modulates collagen fibrillogenesis. Biomacromolecules 9:2562–2566, 2008. [PubMed: 18680341]
50. Paderi JE, Sistiabudi R, Ivanisevic A, and Panitch A. Collagen-binding peptidoglycans: a biomimetic approach to modulate collagen fibrillogenesis for tissue engineering applications. Tissue Eng. Part A 15:2991–2999, 2009. [PubMed: 19323607]
51. Quan BD, and Sone ED. Structural changes in collagen fibrils across a mineralized interface revealed by cryo-TEM. Bone 77:42–49, 2015. [PubMed: 25892483]
52. Raub CB, Putnam AJ, Tromberg BJ, and George SC. Predicting bulk mechanical properties of cellularized collagen gels using multiphoton microscopy. Acta Biomater. 6:4657–4665, 2010. [PubMed: 20620246]
53. Raub CB, Suresh V, Krasieva T, Lyubovitsky J, Mih JD, Putnam AJ, Tromberg BJ, and George SC. Noninvasive assessment of collagen gel microstructure and mechanics using multiphoton microscopy. Biophys. J 92:2212–2222, 2007. [PubMed: 17172303]
54. Rodríguez-Cabello JC, de Torre IG, Ibañez-Fonseca A, and Alonso M. Bioactive scaffolds based on elastin-like materials for wound healing. Adv. Drug Deliv. Rev 129:118–133, 2018. [PubMed: 29551651]
55. Ryan AJ, and O’Brien FJ. Insoluble elastin reduces collagen scaffold stiffness, improves viscoelastic properties, and induces a contractile phenotype in smooth muscle cells. Biomaterials 73:296–307, 2015. [PubMed: 26431909]

56. Schmitt FO, Hall CE, and Jakus MA. Electron microscope investigations of the structure of collagen. J. Cell. Comp. Physiol 20:11–33, 1942.
57. Sharma S, Panitch A, and Neu CP. Incorporation of an aggrecan mimic prevents proteolytic degradation of anisotropic cartilage analogs. Acta Biomater. 9:4618–4625, 2013. [PubMed: 22939923]
58. Sherlock BE, Harvestine JN, Mitra D, Haudenschild A, Hu J, Athanasiou KA, Leach JK, and Marcu L. Nondestructive assessment of collagen hydrogel cross-linking using time-resolved autofluorescence imaging. J. Biomed. Opt 23:036004, 2018.
59. Sionkowska A, Skopinska-Wisniewska J, Gawron M, Kozlowska J, and Planecka A. Chemical and thermal cross-linking of collagen and elastin hydrolysates. Int. J. Biol. Macromol 47:570–577, 2010. [PubMed: 20713081]
60. Stuart K, and Panitch A. Influence of chondroitin sulfate on collagen gel structure and mechanical properties at physiologically relevant levels. Biopolymers 89:841–851, 2008. [PubMed: 18488988]
61. Stuart K, and Panitch A. Characterization of gels composed of blends of collagen l, collagen III, and chondroitin sulfate. Biomacromolecules 10:25–31, 2009. [PubMed: 19053290]
62. Vats K, and Benoit DSW. Dynamic manipulation of hydrogels to control cell behavior: a review. Tissue Eng. Part B 19:455–469, 2013.
63. Vázquez-Portalatín N, Kilmer CE, Panitch A, and Liu JC. Characterization of collagen type I and II blended hydrogels for articular cartilage tissue engineering. Biomacromolecules 17:3145–3152, 2016. [PubMed: 27585034]
64. Vining KH, and Mooney DJ. Mechanical forces direct stem cell behaviour in development and regeneration. Nat. Rev. Mol. Cell Biol 18:728–742, 2017. [PubMed: 29115301]
65. Yankelevich DR, Ma D, Liu J, Sun Y, Sun Y, Bec J, Elson DS, and Marcu L. Design and evaluation of a device for fast multispectral time-resolved fluorescence spectroscopy and imaging. Rev. Sci. Instrum 85:034303, 2014. [PubMed: 24689603]
66. Yao ES, Zhang H, Chen YY, Lee B, Chew K, Moore D, and Park C. Increased β1 integrin is associated with decreased survival in invasive breast cancer. Cancer Res. 67:659–664, 2007. [PubMed: 17234776]
67. Yeo GC, Mithieux SM, and Weiss AS. The elastin matrix in tissue engineering and regeneration. Curr. Opin. Biomed. Eng 6:27–32, 2018.

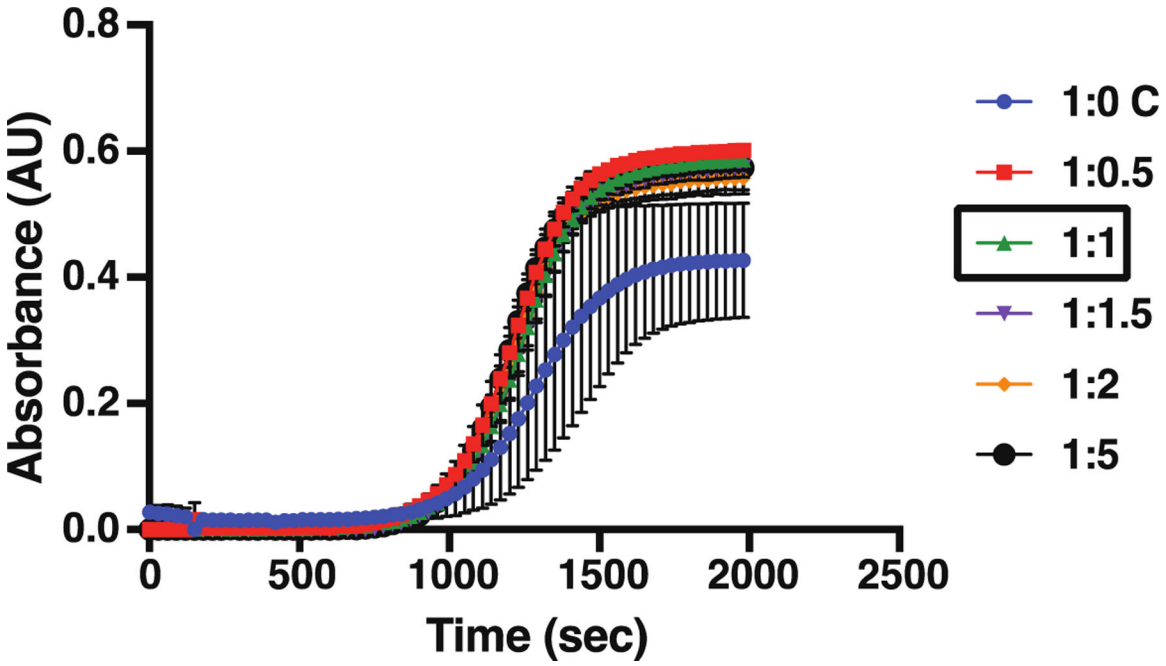

Figure 1.

Turbidity measurements during fibrillogenesis for collagen and elastin blend gel solutions. Addition of elastin significantly increases fibrillogenesis ($p < 0.05$). Data represents mean ± standard deviation (n = 3).

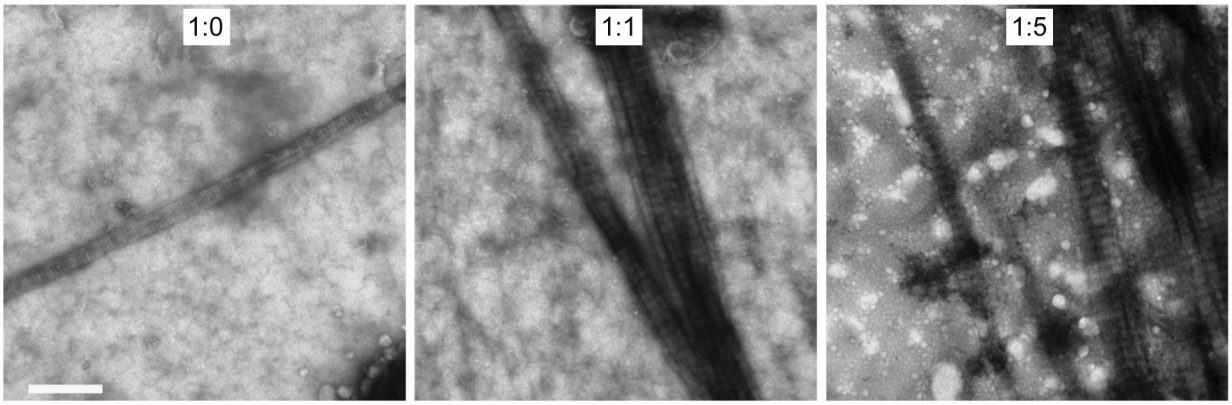

Figure 2.
Representative TEM images of collagen fibrils observed in 1:0 C, 1:1, and 1:5 collagen and elastin blend gels. TEM images were used to measure D-banding pattern length and fibril diameter. Scale bar: 500 nm.

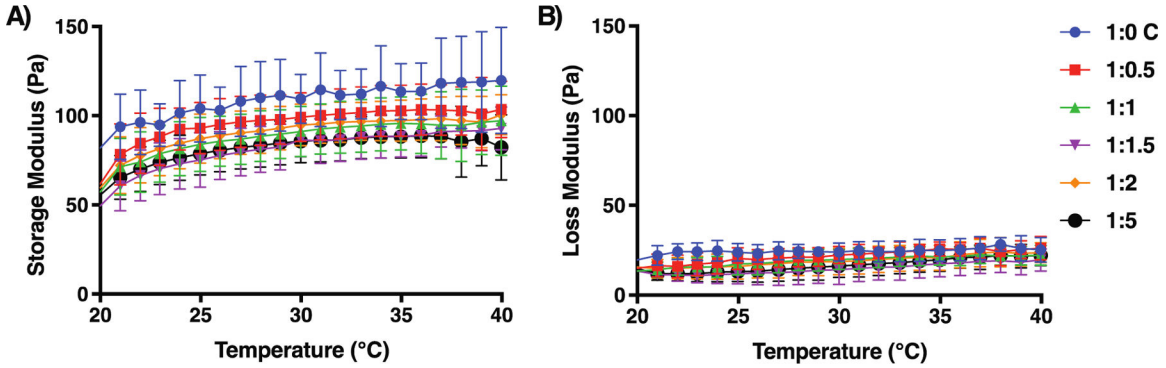

Figure 3.

A) Storage moduli and B) loss moduli of gels prepared from mixtures of 1:0 C, 1:0.5, 1:1, 1:1.5, 1:2, and 1:5 collagen type I to elastin. Data (n = 16–18) are represented as the mean ± the standard deviation.

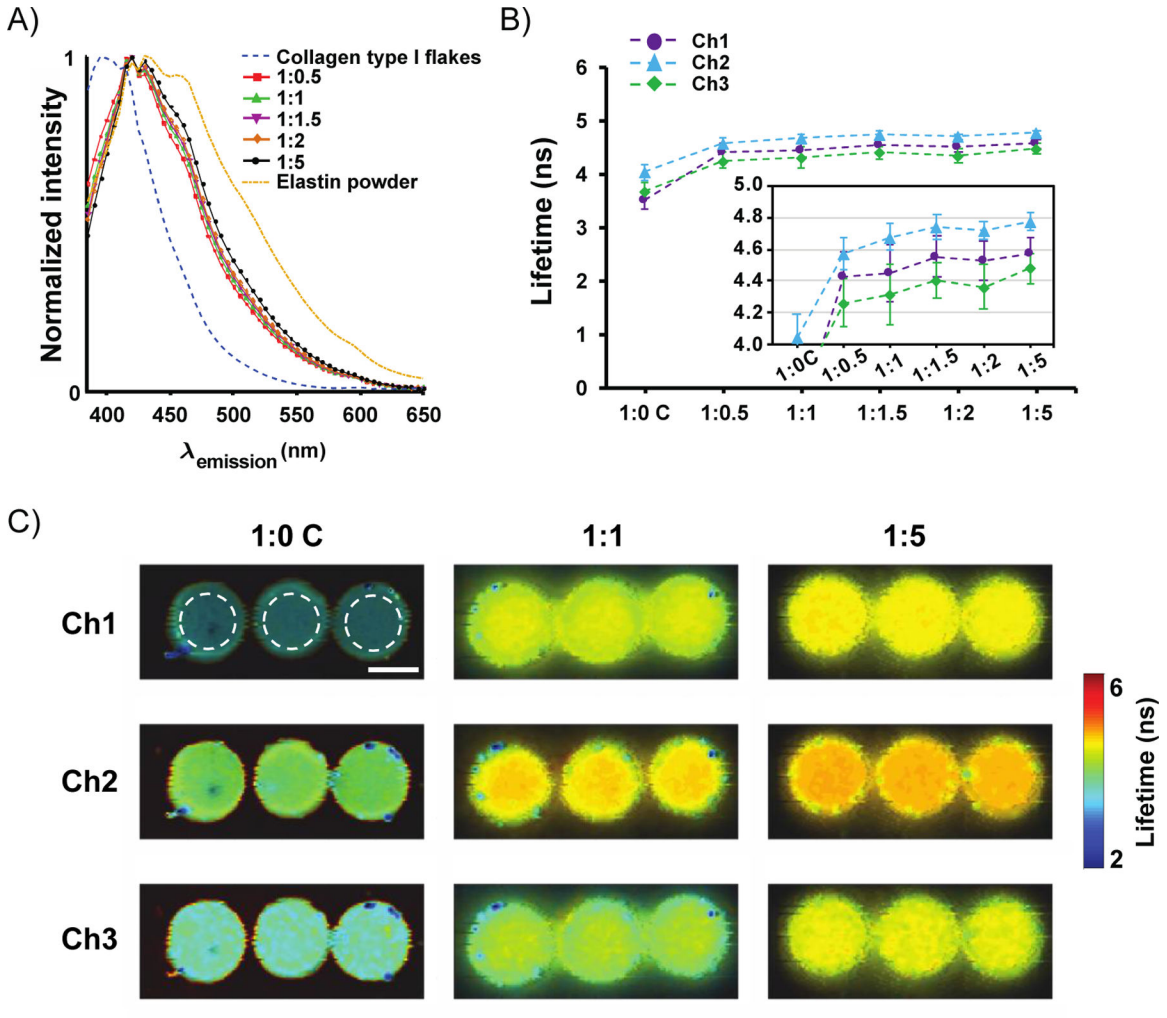

Figure 4.

A) Spectral emission of collagen type I flakes, elastin powder, and the collagen-elastin hydrogel blends at ratios 1:0.5, 1:1, 1:1.5, 1:2, and 1:5. B) Average fluorescence lifetime of the hydrogels. Points and error bars represent mean and standard deviation of lifetime values from pixels within a central and circular ROI (examples in Ch1–1:0C in C) from all n = 9 gels per group. C) Autofluorescence lifetime maps for groups 1:0 C, 1:1, and 1:5 in channels 1 (ch1), 2 (ch2), and 3 (ch3). Scale bar = 5 mm.

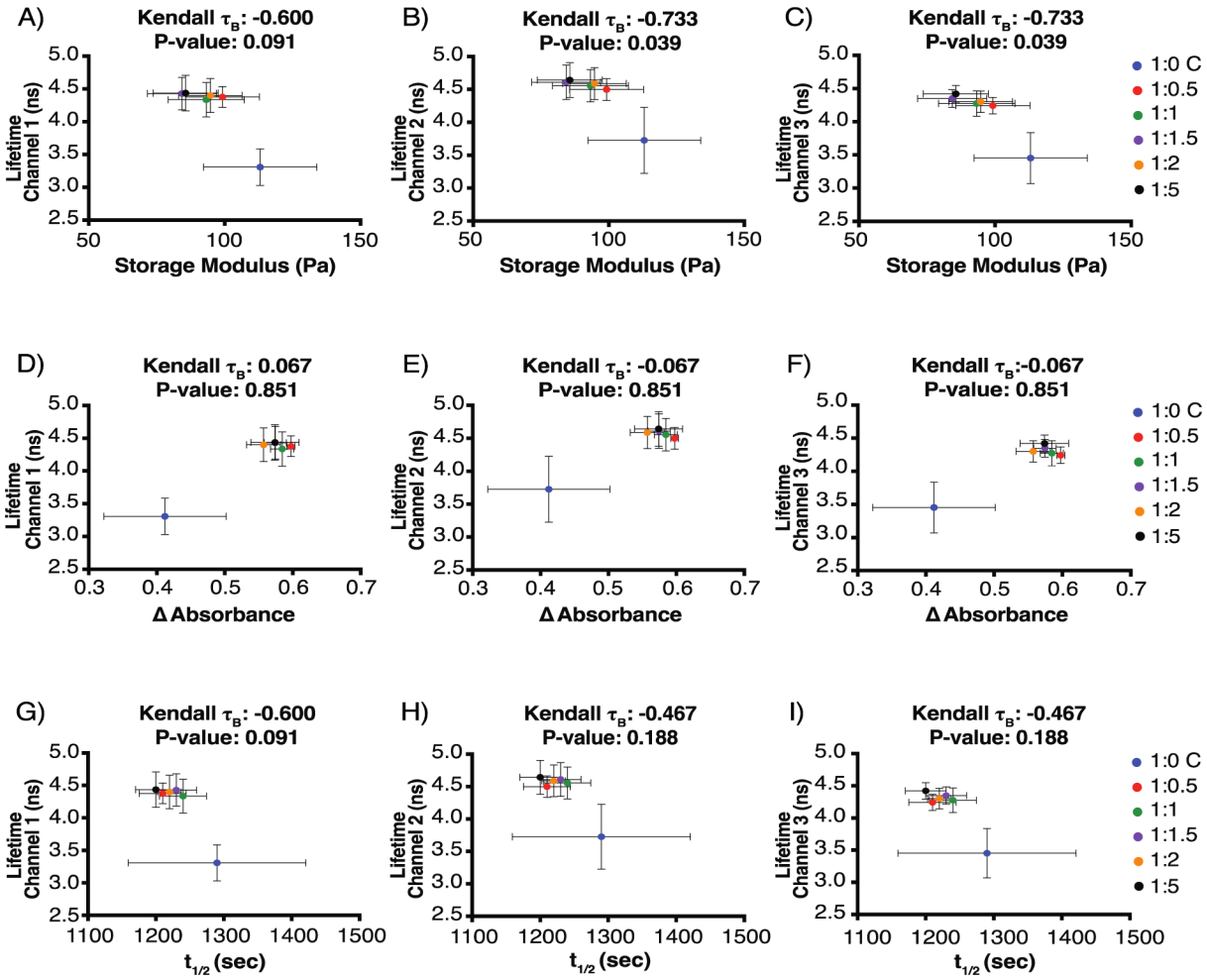

Figure 5.

Correlations between lifetime and storage moduli for (A) Channel 1 (390/18 nm), (B) Channel 2 (435/40 nm), and (C) Channel 3 (542/20 nm). Correlations between lifetime and Δ absorbance for (D) Channel 1, (E) Channel 2, and (F) Channel 3. Correlations between lifetime and halftime ($t_{1/2}$) for (G) Channel 1, (H) Channel 2, and (I) Channel 3 for gels prepared from mixtures of 1:0 C, 1:0.5, 1:1, 1:1.5, 1:2, and 1:5 collagen type I to elastin. The Kendall τ_b coefficient and the *p* value for each combination are shown in the plots. Data (n = 6–13) are represented as the mean ± the standard deviation.

Table 1.

Concentration of collagen type I and elastin in the hydrogels.

Gel Ratio	Collagen (mg/mL)	Elastin (mg/mL)
1:0 C	3.6	0
1:0.5	3.6	1.8
1:1	3.6	3.6
1:1.5	3.6	5.4
1:2	3.6	7.2
1:5	3.6	18

Table 2.

Δabsorbance and halftime measurements for collagen and elastin blend gels.

		Fibrillogenesis			
Gel Type	**N**	**Δ Absorbance (AU) (Mean ± SD)**	**P value**	**Halftime (sec) (Mean ± SD)**	**P value**
1:0 C	3	0.41 ± 0.09		1290 ± 131	
1:0.5	3	0.60 ± 0.01	0.0007	1210 ± 35	0.3850
1:1	3	0.58 ± 0.02	0.0012	1240 ± 35	0.7619
1:1.5	3	0.57 ± 0.02	0.0020	1230 ± 30	0.6305
1:2	3	0.56 ± 0.02	0.0047	1220 ± 17	0.5009
1:5	3	0.57 ± 0.04	0.0021	1200 ± 30	0.2885

One-way ANOVA and Dunnett's method for comparisons with control were performed.

SD: Standard Deviation.

Table 3.

Average D-banding pattern length and fibril diameter for fibrils observed in the collagen and elastin hydrogels.

		D-banding Pattern		Fibril Diameter	
Gel Type	**N**	**Length (nm) (Mean ± SD)**	**P value**	**Diameter (nm) (Mean ± SD)**	**P value**
1:0 C	62	68.15 ± 1.58		70.62 ± 18.44	
1:1	46	68.25 ± 1.99	0.9409	72.32 ± 15.04	0.8740
1:5	48	67.30 ± 2.09	0.0366	68.90 ± 18.25	0.8035

One-way ANOVA and Dunnett's method for comparisons with control were performed.

SD: Standard Deviation.

Table 4.

Average storage moduli and standard deviation values for collagen and elastin blend gels at 30°C.

		Storage Moduli	
Gel Type	**N**	**Storage Modulus (Pa) (Mean ± SD)**	**P value**
1:0 C	17	109.4 ± 13.8	
1:0.5	17	99.2 ± 13.7	0.0807
1:1	16	91.2 ± 14.0	0.0039
1:1.5	16	86.4 ± 9.5	0.0003
1:2	18	94.8 ± 11.7	<0.0001
1:5	18	85.7 ± 12.0	<0.0001

One-way ANOVA and Dunnett's method for comparisons with control were performed.

SD: Standard Deviation.

Table 5.

Autofluorescence lifetimes for the hydrogels.

Gel Type	Channel 1			Channel 2			Channel 3		
	Number of Pixels	Lifetime (ns) (Mean ± SD)	P value	Number of Pixels	Lifetime (ns) (Mean ± SD)	P value	Number of Pixels	Lifetime (ns) (Mean ± SD)	P value
1:0 C	3385	3.52 ± 0.17		3384	4.04 ± 0.15		3378	3.70 ± 0.16	
1:0.5	4521	4.42 ± 0.16	<0.0001	4485	4.57 ± 0.10	<0.0001	4517	4.26 ± 0.15	<0.0001
1:1	4636	4.45 ± 0.18	<0.0001	4628	4.68 ± 0.09	<0.0001	4636	4.32 ± 0.19	<0.0001
1:1.5	4942	4.56 ± 0.13	<0.0001	4864	4.74 ± 0.08	<0.0001	4941	4.41 ± 0.11	<0.0001
1:2	4372	4.53 ± 0.12	<0.0001	4313	4.72 ± 0.05	<0.0001	4372	4.37 ± 0.14	<0.0001
1:5	5498	4.58 ± 0.09	<0.0001	5502	4.78 ± 0.05	<0.0001	5525	4.48 ± 0.09	<0.0001

One-way ANOVA and Dunnett's method for comparisons with control were performed.

N = 9 for all gel types.

SD: Standard Deviation.